Nonmonotonic variation with salt concentration of the second virial coefficient in protein solutions

E. Allahyarov,[1] H. Löwen,[2] J. P. Hansen,[3] and A. A. Louis[3]
[1]*Institut für Festkörperforschung, Forschungszentrum Jülich, D-52425 Jülich, Germany*
[2]*Institut für Theoretische Physik II, Heinrich-Heine-Universität Düsseldorf, D-40225 Düsseldorf, Germany*
[3]*Department of Chemistry, Lensfield Road, Cambridge CB2 1EW, United Kingdom*
(Received 21 February 2003; published 16 May 2003)

The osmotic virial coefficient B_2 of globular protein solutions is calculated as a function of added salt concentration at fixed pH by computer simulations of the ''primitive model.'' The salt and counterions as well as a discrete charge pattern on the protein surface are explicitly incorporated. For parameters roughly corresponding to lysozyme, we find that B_2 first decreases with added salt concentration up to a threshold concentration, then increases to a maximum, and then decreases again upon further raising the ionic strength. Our studies demonstrate that the existence of a discrete charge pattern on the protein surface profoundly influences the effective interactions and that linear and nonlinear Poisson Boltzmann theories fail for large ionic strength. The observed nonmonotonicity of B_2 is compared with experiments. Implications for protein crystallization are discussed.

DOI: 10.1103/PhysRevE.67.051404 PACS number(s): 82.70.Dd, 61.20.Qg, 87.15.Aa

I. INTRODUCTION

Interactions between proteins in aqueous solutions determine their collective behavior, in particular, their aggregation, their complexation with other macromolecules, and ultimately their phase behavior, including phase separation, precipitation, and crystallization. Any theoretical analysis of the properties of protein solutions must rely on a clear understanding of their interactions. A good example is provided by the control of protein crystallization, which is an essential prerequisite for the determination of protein structure by the x-ray diffraction [1,2]. While at present protein crystallization is still mostly achieved experimentally by ''trial and error,'' and on the basis of a number of empirical rules [3], there is clearly a need for a more fundamental understanding of the mechanisms controlling protein crystallization, and this obviously requires a good knowledge of the forces between protein molecules in solution, and of their dependence on solution conditions, including pH and salt concentration [1,4–6].

Protein interactions have various origins, and one may conveniently distinguish between direct and induced (or effective) contributions. Direct interactions include short-range repulsive forces, which control steric excluded volume effects, reflecting the shape of the protein van der Waals dispersion forces, and electrostatic forces associated with pH-dependent electric charges and higher electrostatic multipoles carried by the protein residues [7]. Other, effective, interactions depend on the degree of coarse graining in the statistical description and result from the tracing out of microscopic degrees of freedom associated with the solvent and added electrolyte, i.e., the water molecules and microions. Tracing out the solvent results in hydrophobic attraction and hydration forces, while integrating over microion degrees of freedom leads to screened electrostatic interactions between residues, the range of which is controlled by the Debye screening length, and hence by electrolyte concentration.

However, while coarse graining through elimination of microscopic degrees of freedom, leading to state-dependent effective interactions is *a priori* a reasonable procedure to describe highly asymmetric colloidal systems, where particles have diameters of typically hundreds of nanometers and carry thousands of elementary charges, this is obviously less justified for the much smaller and less charged proteins. In particular, the assumption of uniformly charged colloid surfaces, leading to spherically symmetric, screened interactions between the electric double layers around colloid particles, as epitomized by the classic DLVO (Derjaguin-Landau-Verwey-Overbeek) potential [8], ceases to be a reasonable approximation at the level of nanometric proteins carrying typically of the order of 10 elementary charges. The reason is that length scales that are widely separated in colloidal assemblies, become comparable in protein solutions, while the discreteness of charge distributions on proteins can no longer be ignored, since the distance between two charged residues on the protein surface is no longer negligible compared to the protein diameter. Thus, electrostatic, as well as other (e.g., hydrophobic) interactions are much more specific in proteins, and must be associated with several interaction sites, rather than merely with the centers of mass as is the case for (spherical) colloidal particles.

Another very important distinction between colloids and protein solutions is that the forces between the former may be measured directly, using optical means [9–11], while interactions between proteins can only be inferred indirectly, from measurements by static light scattering of the osmotic equation of state which, at sufficiently low concentrations, yields the second osmotic virial coefficient B_2 [3,12–14], the main focus of the present paper. The variation of B_2 with solution conditions yields valuable information on the underlying effective pair interactions between proteins. Moreover, it was shown empirically by George and Wilson [3] that there is a strong correlation between the measured values of B_2 and the range of solution conditions that favor protein crystallization [12,15,16]. Crystallization can only be achieved if the measured value of B_2 falls within a well defined ''slot.'' If B_2 is too large, repulsive interactions predominate, leading to slow crystallization rates. On the other

hand, if B_2 is highly negative, strong attractions lead to amorphous aggregation.

The correlation between B_2 and crystallization may be rationalized by noting that protein crystals generally coexist with a fairly dilute protein solution, the thermodynamic properties (and, in particular, the free energy) of which are essentially determined by B_2. Coexistence between a dense solid phase and a dilute fluid phase is generally a signature of a very short-ranged attraction between particles as compared to their diameter [16–19].

For such short-ranged attractive interactions, the phase separation into dilute and concentrated proteins solutions expected on the basis of a mean-field van der Waals theory, is in fact preempted by the freezing transition, i.e., the critical (or ''cloud'') point lies below the freezing line. The critical fluctuations associated with this metastable cloud point may lead to a significant enhancement of the crystal nucleation rate [20], while the position of the cloud point in the concentration-temperature plane is strongly correlated with the virial coefficient B_2 [16].

The present paper focuses on the variation of B_2 with ionic strength of added salt. This is a particularly important issue since ''salting out'' of protein solutions is one of the standard methods used to induce crystallization. An increase in salt concentration reduces the screening length and hence the electrostatic repulsion, allowing short-range attractive forces (e.g., of hydrophobic or van der Waals origin) to come into play which will ultimately trigger nucleation. Recent experiments and theoretical considerations point to a nonmonotonic variation of B_2 with increasing ionic strength [21–25], or to a pronounced shoulder in the B_2 versus ionic strength curve [26] in lysozyme solutions. A similar nonmonotonic variation has recently been reported in β-lactoglobulin *A* solutions [27]. Closely related findings are the observation of a nonmonotonic cloud point [28–30], and of a minimum in the solubility of lysozyme with increasing salt concentration [31,32]; the solubility is obviously related to the osmotic virial coefficient [33,34]. Similarly, the attractive interaction parameter λ, which controls the variation of the measured protein diffusion coefficient D with volume fraction, was found to exhibit a sharp minimum upon an increase of ionic strength of lysozyme solutions [35]; again, this interaction parameter strongly correlates with B_2 [36,37].

Traditional models for the protein-protein interaction cannot easily reproduce such nonmonotonic behavior of B_2 or related quantities. The ''colloidal'' approach based on spherical particles interacting via the screened Coulomb DLVO potential [8] can only predict a monotonic decrease of B_2 with ionic strength [5,38]. The same is true for models [5,12,15] accounting for short-range attractions via Baxter's ''adhesive sphere'' representation [39]. In these models, which assume central pairwise interactions, B_2 reduces to a simple integral of the Mayer function associated with the spherically symmetric potential [40,41]. More recent calculations account for the asymmetric shape of proteins [22,42], or include several ''sticky'' sites at the surface of the protein [43,44].

In these traditional calculations, electrostatic interactions between proteins and microions are routinely treated within mean-field Poisson-Boltzmann (PB) theory, generally in its linearized version (as is the case for the classic DLVO potential). However, as explained earlier, all relevant length scales (i.e., protein diameter, mean distance between charged sites on the protein surface, and between coions and counterions, as well as the Debye screening length) are comparable in protein solutions, so that the discrete nature of both the interaction sites, and of the coions and counterions, can no longer be ignored. Moreover, Coulomb correlations are expected to be enhanced on the protein length scales and may lead to strong deviations from the predictions of PB theory, which have recently been shown to induce short-range attractions, even between much larger colloidal particles [28,45–48].

The present paper takes into account the discrete nature of the microions within a ''primitive model'' description of the electrolyte, and presents results of molecular dynamics (MD) calculations of the equilibrium distribution of coions and counterions around two proteins and of the resulting osmotic virial coefficient B_2. Two models of the charge distribution on the surface of the spherical proteins will be considered. In the colloidlike model the charge is assumed to be uniformly distributed over the surface, while in the discrete charge model, the charges are attached to a small number of interaction sites. The latter model will be shown to lead to a distinctly nonmonotonic variation of B_2 with ionic strength, as observed experimentally. During preparation of the current paper, Striolo *et al.* [49] published a study, where similar colloidal models for proteins were considered. They examined a colloid that comprises of discrete charges of both signs to account for nonuniform charge distribution. The simulation results of Ref. [49] show a strong influence of dipolar interactions on effective forces.

The paper is organized as follows. The model and key physical quantities are introduced in Sec. II. Simulation details are described in Sec. III. Results of the simulations are presented and discussed in Sec. IV, while conclusions are summarized in Sec. V. A preliminary account of parts of the results was briefly reported elsewhere [50].

II. MODELS, EFFECTIVE FORCES, AND SECOND VIRIAL COEFFICIENT

The globular proteins under consideration are modeled as hard spheres of diameter σ_p, carrying a total (negative) charge $-Ze$. Within a primitive model representation [51], the molecular granularity of the aqueous solvent is ignored, and replaced by a continuum of dielectric permittivity ϵ, while the monovalent counterions and salt ions are assumed to have equal diameters σ_s and charges $q_s = \pm e$.

Two models are considered for the charge distribution on the surface of the protein. In the ''smeared charge model'' (SCM), the total charge $-Ze$ is assumed to be uniformly distributed over the spherical surface, which is the standard model for charge-stabilized colloidal suspensions [28,45–48], involving highly charged objects. According to Gauss' theorem, the SCM is equivalent to the assumption that the total charge Ze is placed at the center of the sphere. In the

''discrete charge model'' (DCM), point charges $(-e)$ are distributed over a sphere of diameter $\sigma_d = \alpha\sigma_p$, in such a way as to minimize the electrostatic energy of the distribution. Obviously, for very small α, the DCM model will tend to coincide with the SCM model. In practice, the ionized residues are near the protein surface, and the precise choice of α is made according to a Coulomb coupling criterion elaborated at the end of Sec. III. The resulting optimized charge pattern, well known from the classic Thompson problem (see Ref. [52] for a recent review), is kept fixed throughout. Such Thompson patterns do not correspond to the true charge distribution on any specific protein (see Refs. [53,54], where a simple toy model of lysozyme with different charge distribution corresponding to solutions of different pH is constructed) but do provide a well defined discrete model for any value of Z. Note that the discrete distributions are characterized by nonvanishing multipole moments, depending on the symmetry of the distribution for any specific value of Z, while the SCM implies vanishing multipoles of all orders.

At this stage the SCM and DCM models involve only excluded volume and bare Coulomb interactions (reduced by a factor $1/\epsilon$ to account for the solvent) between all particles, proteins as well as microions.

The following physical quantities were systematically computed in the course of the MD simulations, to be described in the following section.

(a) The density profiles of coions and counterions around a single globular protein is defined via

$$\rho_{\pm}(\vec{r}) = \left\langle \sum_j \delta(\vec{r}_j^{\pm} - \vec{r}) \right\rangle. \tag{1}$$

Here, $\vec{r}_j^{\pm}$ is the position of the jth microion of species $\pm$ relative to the protein center, while the angular bracket denotes a canonical average over the microion configurations. For an isolated SCM protein these profiles are spherically symmetric, and depend only on the radial distance $r = |\vec{r}|$. For isolated DCM proteins the profiles are no longer spherically symmetric, and may be expanded in spherical harmonics. The anisotropy turns out to be weak, and only the spherically symmetric component [corresponding to averaging $\rho_{\pm}(\vec{r})$ over protein orientations] will be shown in the following.

(b) The second quantity, which will be the key input in the calculation of B_2, is the microion averaged total force $\vec{F}_1 = -\vec{F}_2$ acting on the centers of two proteins, placed at a relative position $\vec{r} = \vec{r}_1 - \vec{r}_2$; the force $\vec{F}_1$ is a function of $\vec{r}$. Its statistical definition was discussed earlier in the context of charged colloids [45,55,56], and it involves three contributions

$$\vec{F}_1 = \vec{F}_1^{(1)} + \vec{F}_1^{(2)} + \vec{F}_1^{(3)}. \tag{2}$$

$\vec{F}_1^{(1)}$ is the direct Coulomb repulsion between the charge distributions on the two proteins; $\vec{F}_1^{(2)}$ is the microion induced electrostatic force, while $\vec{F}_1^{(3)}$ is the depletion force that may be traced back to the inbalance of the osmotic pressure of the microions acting on the opposite sides of protein 1 due to the presence of protein 2. $\vec{F}_1^{(3)}$ is directly expressible as the integral of the microion contact density over the surface of the protein [57,58].

In the case of the SCM, the microion averaged force depends only on the distance $r = |\vec{r}_{12}|$ between the two proteins. For the DCM, on the other hand, $\vec{F}_1$ is a function of the relative orientations of the two proteins, as characterized by the sets of Euler angles $\vec{\Omega}_1$ and $\vec{\Omega}_2$, i.e., $\vec{F}_1 = \vec{F}_1(\vec{r}, \vec{\Omega}_1, \vec{\Omega}_2)$.

(c) Once the force $\vec{F}_1$ has been determined as a function of $\vec{r}$, $\vec{\Omega}_1$, and $\vec{\Omega}_2$, one may then calculate an orientationally averaged, but distance resolved, effective protein-protein pair potential according to

$$V(r) = \int_r^{\infty} dr' \left\langle \frac{\vec{r}'}{|\vec{r}|} \cdot \vec{F}_1(\vec{r}', \vec{\Omega}_1, \vec{\Omega}_2) \right\rangle_{\vec{\Omega}_1, \vec{\Omega}_2}, \tag{3}$$

where the angular brackets $\langle \cdots \rangle_{\vec{\Omega}_1 \vec{\Omega}_2}$ refer to a canonical statistical average over mutual orientations of the two proteins weighted by the Boltzmann factor of the effective potential $V_{eff}(\vec{r}, \vec{\Omega}_1, \vec{\Omega}_2)$ such that $\partial V_{eff}(\vec{r}, \vec{\Omega}_1, \vec{\Omega}_2)/\partial \vec{r} = -\vec{F}_1(\vec{r}, \vec{\Omega}_1, \vec{\Omega}_2)$. Explicitly, for any quantity $A(\vec{r}, \vec{\Omega}_1, \vec{\Omega}_2)$,

$$\langle A \rangle_{\vec{\Omega}_1, \vec{\Omega}_2} = \frac{\int d\vec{\Omega}_1 d\vec{\Omega}_2 A(\vec{r}, \vec{\Omega}_1, \vec{\Omega}_2) \exp\{(-V_{eff}(\vec{r}, \vec{\Omega}_1, \vec{\Omega}_2)/k_B T)\}}{\int d\vec{\Omega}_1 d\vec{\Omega}_2 \exp\{-V_{eff}(\vec{r}, \vec{\Omega}_1, \vec{\Omega}_2)/k_B T\}}. \tag{4}$$

In practice, the anisotropy of V_{eff} turns out to be sufficiently weak so as to justify an unweighted angular average in Eq. (4), i.e., to set the Boltzmann factor equal to 1.

(d) The second virial coefficient B_2 finally follows from the expression

$$B_2 = \frac{1}{2} \int d\vec{r}[1 - b(r)], \tag{5}$$

where

$$b(r)=\left(\frac{1}{8\pi^2}\right)^2\int d\vec{\Omega}_1 d\vec{\Omega}_2 \exp[-V_{eff}(\vec{r},\vec{\Omega}_1,\vec{\Omega}_2)/k_BT]. \tag{6}$$

The angular integrations are trivial in the case of the SCM, where V_{eff} depends only on r. In the case of the DCM, one may use the identity

$$b(r)=\exp\left[-\int_r^\infty dr'\frac{d}{dr'}[\ln b(r')]\right], \tag{7}$$

to show that B_2 may be cast in a form similar to that appropriate for the SCM, namely,

$$B_2=\frac{1}{2}\int d\vec{r}[1-\exp\{-V(r)/k_BT\}], \tag{8}$$

where $V(r)$ is the potential of the orientationally averaged projected force, as defined in Eq. (3). As pointed out earlier, B_2 is directly accessible experimentally by extrapolating light scattering data to small wave vectors [41] or by taking derivatives of osmotic pressure data with respect to concentration [13,14]. Results will be presented in the form of the reduced second virial coefficient $B_2^*=B_2/B_2^{(HS)}$, where $B_2^{(HS)}=2\pi\sigma_p^3/3$, i.e.,

$$B_2^*=1+\frac{3}{\sigma_p^3}\int_{\sigma_p}^\infty r^2 dr[1-\exp\{-V(r)/k_BT\}]. \tag{9}$$

III. SIMULATION DETAILS

We study a pair ($N_p=2$) of spherical proteins with center-to-center separation r, confined in a cubic box of length $L=4\sigma_p$, which also contained monovalent coions and counterions in numbers determined by their bulk concentrations and overall charge neutrality. There are ZN_p counterions dissociated from the protein surface, and N_s added salt ion pairs such that the screening of proteins is due to $N_+=N_s$ coions and $N_-=N_s+ZN_p$ counterions in the simulation box. A snapshot of a typical equilibrium microion configuration around two proteins is shown in Fig. 1 for the protein charge number $Z=15$. The two proteins were placed symmetrically with respect to the center along the body diagonal of a cubic simulation cell; periodic boundary conditions in three dimensions were adopted. L was chosen such that the box length is much larger than the range of the total (effective) protein-protein interaction, so that the results are independent of L for nonzero salt concentration. The long-range electrostatic interactions between two charged particles in the simulation box with periodic boundary conditions were modified using the Lekner summation method of images [59]. For our model to be a rough representation of lysozyme, we chose $\sigma_p=4$ nm, and three different protein charges $Z=6$,10, and 15, corresponding to three different values of the solution pH. The microion diameter was chosen to be $\sigma_c=\sigma_p/15=0.267$ nm.

For both the SCM and the DCM, the contact coupling parameter between a protein and a microion, namely, $\Gamma=2e^2/[\epsilon k_BT(\sigma_p-\sigma_d+\sigma_c)]$ for the DCM, and $\Gamma=2Ze^2/[\epsilon k_BT(\sigma_p+\sigma_c)]$ for the SCM, are comparable, and of the order of $\Gamma\approx 3$ at room temperature. We fixed the dielectric constant of water to be $\epsilon=81$ and the system temperature to be $T=298$ K. Varying salt concentration for fixed protein charge Z corresponds to a fixed solution pH [60].

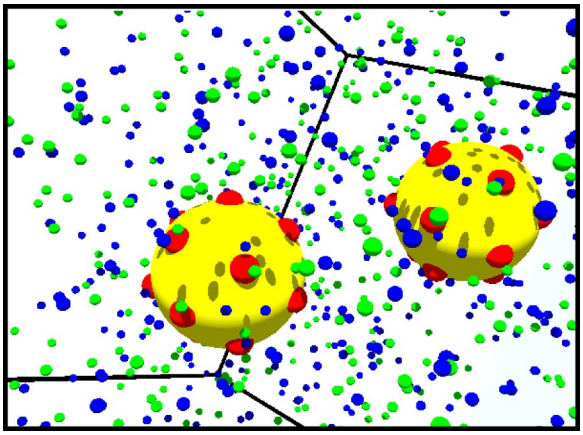

FIG. 1. Snapshot of a typical MD-generated microion configuration around two proteins, separated by $r=1.7\sigma_p$. The proteins carry 15 discrete charges $-e$ and the monovalent salt density is $C_s=0.206$ mol/l. The globular protein molecules are shown as two large gray spheres. The embedded small dark spheres on their surface mimic the discrete protein charges in the DCM model. The small gray spheres are counterions, while the black spheres are coions.

Details of the runs corresponding to different salt concentrations are summarized in Table I. Note that the Debye screening length r_D, defined by

$$r_D=\sqrt{\frac{\epsilon k_BTV}{8\pi(N_s+Z)q_se^2}} \tag{10}$$

is less than 10 Å for salt concentration beyond 0.1 M. Here, V is the accessible volume for salt ions such that the salt

TABLE I. Parameters used for the different simulation runs. N_s is the number of salt ion pairs in simulation box, C_s is the salt concentration in mol/l, the Debye screening length r_D is defined by Eq. (10), and $r_s=(3V/4\pi(2N_s+2Z))^{1/3}$ is the average distance between salt ions for a given salt concentration.

Run	N_s	C_s (mol/l)	r_D/σ_p	r_s/σ_p
1	0	0	0	0
2	125	0.05	0.34	0.39
3	250	0.103	0.24	0.31
4	500	0.206	0.17	0.25
5	1000	0.412	0.12	0.2
6	1500	0.62	0.1	0.17
7	2000	0.824	0.085	0.16
8	2500	1.03	0.077	0.15
9	3000	1.24	0.07	0.14
10	4000	1.65	0.06	0.124
11	5000	2.061	0.054	0.118

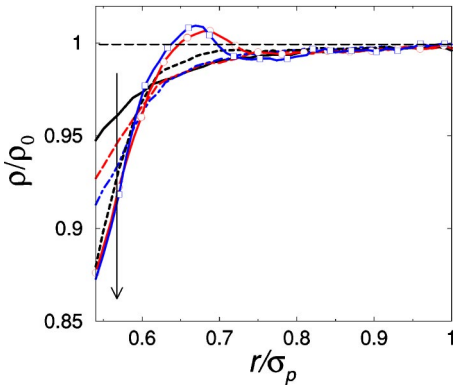

FIG. 2. Normalized total salt density profiles $\rho(r)$ near a single *neutral sphere*. $\rho_0 = N_s/V$ is the bulk density. The added salt concentration is increased from top to bottom (see the arrow, which refers to the density near the protein surface) according to runs 1–5, 7, 9.

concentration C_s is N_s/V. Thus, the point charges on the protein surface are effectively screened from each other [29]. For each of the runs indicated in Table I, the distance-resolved effective forces and interaction potentials are calculated according to Eqs. (2) and (3). The statistical averages over microion configurations leading to $\vec{F}_1^{(2)}$ and $\vec{F}_1^{(3)}$ were evaluated from time averages in the MD simulations.

IV. MICROION DISTRIBUTIONS AROUND A SINGLE PROTEIN

First, as a reference, consider a single protein ($N_p = 1$) placed at the center of the simulation box. We calculated spherically averaged, radial microion density profiles $\rho(r) = \rho_+(r) + \rho_-(r)$ in the immediate vicinity of the protein surface. For a single *neutral* sphere in a salted solution, results for $\rho(r)$ are drawn in Fig. 2. There is a marked depletion in the microion density, signaled by a minimum of $\rho(r)$ at contact, well below the asymptotic bulk value. For low salt concentration, the observed depletion zone of salt ions around a neutral sphere is in qualitative agreement with the standard analysis based on the linearized theory which involves a correction $\sim -\exp(-2r/r_D)/r^2$ [61] to the homogeneous density. The depletion is enhanced upon increasing the salt concentration. At sufficiently high salt concentrations, this minimum is followed by a weak, but detectable, ion layer (see corresponding lines for runs 7 and 9 in Fig. 2). The formation of a depletion zone is *not* a consequence of the direct (hard-core) interaction between salt ions and the protein surface, since the position of the observed layer is significantly further away from the protein surface than one ion diameter. A rough estimate for the distance between layer and neutral sphere gives a value of $2.5\sigma_s$, or equivalently $0.17\sigma_p$. For runs 7 and 9, where the ion layer emerges, this distance is of the order of an average ion separation r_s in the system and twice the Debye screening length r_D as well (see Table I). Obviously, it is the small ion correlations that lead to the peak formation in the salt density profiles. An intuitive argument is that the lack of mutual polarization in a dense salt solution near neutral surfaces causes ion depletion. The

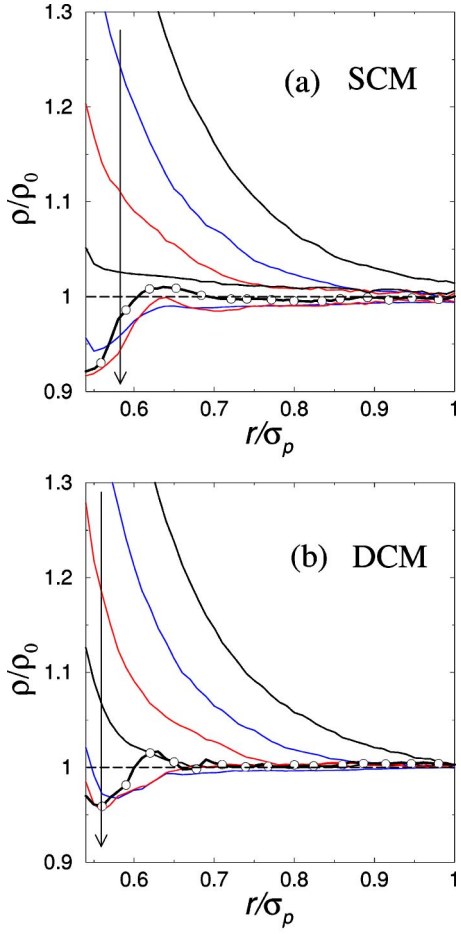

FIG. 3. Total salt density near a single protein surface for the SCM (a) and the DCM (b) models and runs 2–5, 7, 9, 11. The arrow (in the direction of an increase in added salt concentration) applies to all runs except run 11, which is shown as a solid line with symbols.

physical meaning of this depletion is discussed in more detail in Ref. [61]. Qualitatively similar depleted density profiles were observed in Lennard-Jones system confined between neutral planes [62] and in Yukawa mixtures [63]. Furthermore, an effective force that pushes a single ion towards regions of higher salinity is predicted within Debye-Hückel theory for interfacial geometries [64].

Next we consider a protein sphere with charge number $Z = 10$. The total salt densities, as sums of coions and counterion densities, are shown in Fig. 3 for both the SCM and DCM. At the lower salt concentrations (up to run 5) the SCM and DCM models both yield an accumulation of the microion density near ion-protein contact, in semiquantitative agreement with the prediction of standard PB theory. For rising ionic strength, the total microion density gets depleted near the protein surfaces, as in the previously considered case of a neutral sphere. Remarkably, this depletion occurs both with the SCM and DCM and contradicts the PB prediction. The intuitive picture is that a microscopic layer of counterions is formed around the proteins. An additional salt pair now profits more from the bulk polarization than from the protein surface polarization and is thus excluded from this

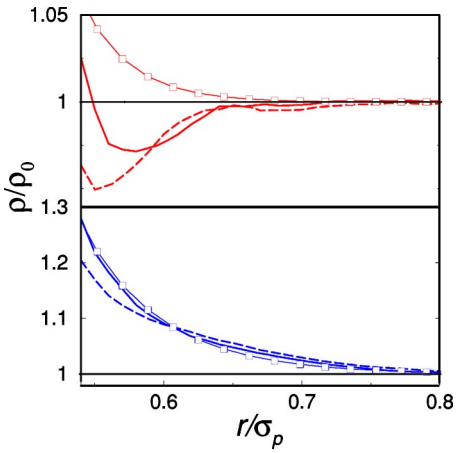

FIG. 4. Total density profiles $\rho(r)$ of salt ions around a single protein with $Z=10$, for run 4 (bottom set of curves) and run 7 (upper set of curves), comparing the DCM simulations (solid line), the SCM simulations (dashed line), and nonlinear Poisson-Boltzmann theory of the SCM (squares connected by lines).

layer. By normalizing the profiles to the total bulk density, this effect becomes visible as a depletion zone in Fig. 3, where a noticeable difference between the SCM and DCM profiles also emerges. Whereas the DCM predicts a contact value $\rho_c(r=(\sigma_p+\sigma_c)/2)$ larger than the bulk value, the SCM predicts a much stronger microion depletion near contact. More generally, the contact value of the DCM model is always larger than that of the SCM model for the same salt concentrations. This finding illustrates the sensitivity of correlation effects to the assumed charge pattern at the surface of a protein. This correlation effect is, of course, absent in linear and nonlinear PB theories, which always predict a monotonically decreasing density profile $\rho(r)$. A direct comparison between the SCM, DCM models and nonlinear PB theory solved in a spherical cell within the SCM [65] is shown in Fig. 4 for two of the higher salt concentrations from Fig. 3. For the intermediate salt concentration $C_s=0.206$ mol/l (run 4) both simulation and theory predict a monotonic decrease of salt density away from the protein surface. Surprisingly, the PB result for the SCM is in good agreement with the simulation result for the DCM. This tendency is observed up to run 5, we believe that it is due to an artificial cancellation of errors in the PB treatment of small ion densities. It is a well known fact that near a colloidal surface the PB densities are higher than the simulated ones for the traditional SCM colloids. On the other hand, the DCM densities are systematically larger than the SCM results at ion-protein contact, as shown in Fig. 3. As a result, the PB results turn out to be closer to the DCM than to the SCM densities. In the case of the higher salt concentration, $C_s=0.824$ mol/l (run 7), the simulation results strongly deviate from the PB predictions. Note that the long-range behavior of the concentration profiles is not well reproduced by the PB cell model. A comparison between the SCM and DCM results for run 7 (solid and dashed lines in Fig. 4) reveals a strong colloidal charge-counterion pair association for the DCM. This result is in accordance with the findings of Ref. [66], where a significant influence of the colloid charge discretization on the counterion distribution is revealed.

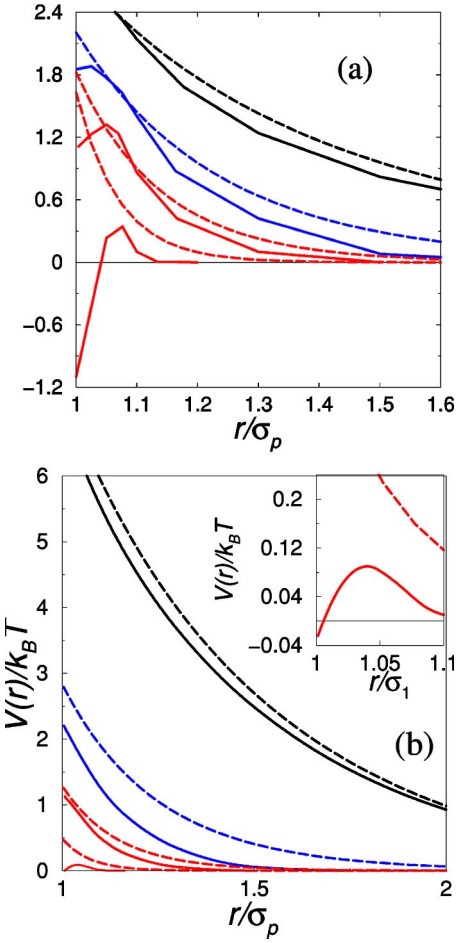

FIG. 5. Total force $F(r)$ (a) and interaction potential $V(r)$ (b) versus dimensionless distance r/σ_p within the SCM, for a protein charge $Z=10$. The force is divided by $F_0=k_BT/\lambda_B$, where $\lambda_B=e^2/\epsilon k_BT$ is the Bjerrum length. The added salt concentration increases from top to bottom, according to runs 1, 3, 5, 11. Dashed lines correspond to the DLVO theory. The inset in (b) shows in more detail the differences between the SCM simulations and the DLVO potential for run 11.

A multipole expansion of the total salt number density in the DCM, demonstrates that the higher order expansion coefficients are strongly damped and much weaker than the zero-order homogeneous term shown in Figs. 3 and 4.

Effective force and B_2 for a protein pair

Next we consider the angularly averaged effective force $F(r)=-dV(r)/dr$ and potential $V(r)$ between two proteins embedded in a sea of small salt ions. Simulation results for the simpler case of the SCM are plotted in Fig. 5 for $Z=10$ and compared with the DLVO theory. There is a systematic deviation between the theoretical and simulation results. While the DLVO [8] potential

$$U^{(DLVO)}(r)=\frac{Z_{DLVO}^2e^2}{\epsilon r}\exp(-r/r_D), \tag{11}$$

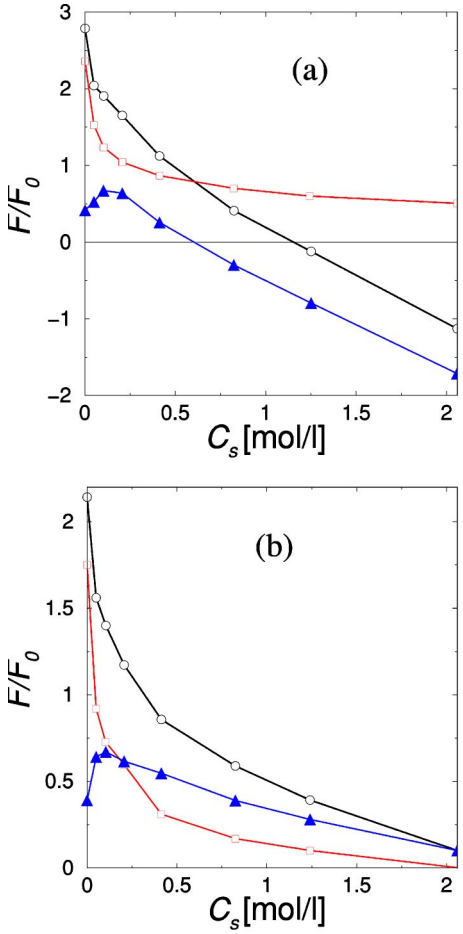

FIG. 6. The total force F (circles) and its electrostatic $F^{(2)}$ (squares) and entropic $F^{(3)}$ (triangles) components versus salt concentration. The separation distance is fixed at (a) $r/\sigma_p=1$ and (b) $r/\sigma_p=1.1$. The simulations are for the SCM with $Z=10$, and show that at high salt concentrations, the entropic force dominates.

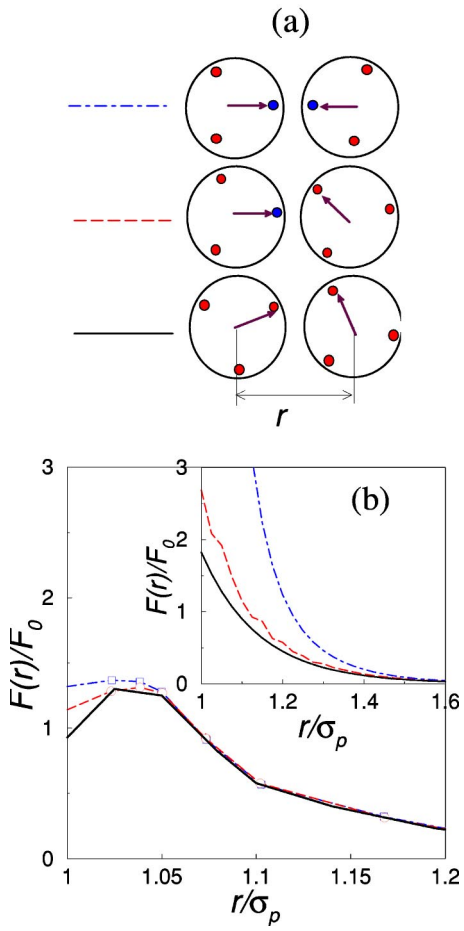

FIG. 7. (a) An illustration of three different mutual orientations of two proteins. Points inside spheres represent protein charges in the DCM. (b) Total interaction force $F(r)$ versus dimensionless separation distance r/σ_p for mutual orientations shown in (a) for run 5 and $Z=10$ in the DCM. The inset shows the same, but for a Yukawa segment model.

where $Z_{DLVO}=Z\exp[(\sigma_p+\sigma_c)/2r_D]/[1+(\sigma_p+\sigma_c)/2r_D]$, always results in a repulsive force, the simulations indicate the possibility of an attraction between proteins for large salt concentrations. The force $F(r)$ at the higher salt concentrations C_s shows a maximum at a distance r nearly equal to the ion diameter. Note that, for the highest salt concentration considered, $C_s=2.061$ mol/l (run 11), where the electrostatic interactions are almost completely screened out, the effective force $F(r)$ is dominated by entropic effects, see also the inset in Fig. 5(b); it is reminiscent of the entropic depletion force of hard sphere system. The corresponding potential is negative at short distances, as shown in the inset of Fig. 5(b), and is related to the depletion in the microion total density profiles $\rho(r)$ around an isolated protein, shown in Fig. 3. We note that such an entropic attraction is not contained in DLVO theory. Its origin is also different from the salting-out effect studied in Refs. [12,67–70] or the macroion overcharging effect studied in Ref. [71]. In Fig. 6, the salt dependence of the total interaction force $F(r)$ [Eq. (2)] is broken up into its components $F^{(2)}$ and $F^{(3)}$ for two values of r. This helps to show that at large salt concentrations it is indeed the entropic component that causes the force to be attractive for run 11 in Figs. 5(a) and 6(a). Finally, we mention that the range of attraction observed here will depend on the electrolyte (salt ion) size [72]. This feature of our model may hint at a cause for the salt specificity observed in salting-out experiments on protein crystallization [73].

The same calculations were carried out for the other two protein charges in the SCM model, $Z=6$ and $Z=15$, with qualitatively similar results to those obtained for $Z=10$. For all charges and salt densities considered, the long-range behavior of interaction forces and potentials is always in poor quantitative agreement with the DLVO predictions. For a better match of theory and simulation, one would have to carry out an additional rescaling procedure of the bare protein charge Z [in Eq. (11)].

It is clear that the effective forces and potentials between two proteins will no longer be spherically symmetric within the DCM model. Three distinguishable mutual orientations of the two proteins are schematically outlined in Fig. 7(a), corresponding to particular configurations of the Euler angles $\vec{\Omega}_1,\vec{\Omega}_2$ of the two proteins. Nevertheless, our simulation results, presented in Fig. 7(b), for these three orientations,

show that the actual force anisotropy is weak. This observation justifies *a posteriori* the assumption made in Eq. (4), where the angular-dependent Boltzmann weight was set to one. However, this is no longer true for the Yukawa segment model [56,74,75], as shown in the inset of Fig. 7(b). Within this model, the total effective interaction potential between a pair of proteins is given by

$$U^{(YS)}(r)=\frac{1}{Z^2}\sum_{n,k=1}^{Z} U^{(DLVO)}(|\vec{r}_k^{(1)}-\vec{r}_n^{(2)}|), \qquad (12)$$

where $\vec{r}_k^{(1)}$ and $\vec{r}_n^{(2)}$ represent the positions of the point unit charges on different proteins. We emphasize that the aelotopic (or nonisotropic) interactions incorporated in our DCM differ from those considered, for example, in Ref. [44], where B_2 is calculated for a set of hydrophobic *attractive* patches on the protein surface. Within our version of the DCM the third configuration in Fig. 7(a) (solid line), has the highest statistical weight of the three cases shown [see Eqs. (3) and (4)]. If, on the other hand, the point charges on the protein are replaced by attractive patches [44], then the configuration with two points nearly touching [dot-dashed line in Fig. 7(a)], is the statistically most favorable conformation. Similar arguments hold within a molecular model for site-specific short-range attractive protein-protein interactions [76,77]. Results for distance-resolved forces within the DCM model are shown in Fig. 8(a), for $Z=10$. When the salt concentration is less than $C_s \lesssim 0.2$ mol/l, the results are similar to those of the SCM model: i.e., for low ionic strength, the force is repulsive, while for high ionic strength there is an attraction near contact followed by a repulsive barrier. The distinguishing property of the DCM is the *nonmonotonicity* of the force with the increase of ionic strength. This, in turn, gives rise to the nonmonotonic behavior of the spherically averaged interaction potential $V(r)$ shown in Fig. 8(b). This feature of $V(r)$ manifests itself in the following way in Fig. 8(b): the potential is first strongly reduced as C_s is increased, then its amplitude and range increase very significantly at intermediate concentrations ($C_s \simeq 1$ mol/l), before it nearly vanishes at the highest salt concentrations. Note that $V(r)$ even becomes slightly attractive at contact ($r=\sigma_p$) for $C_s \simeq 2$ mol/l. Similar effects are also observed for $Z=6$ and $Z=15$ (see Fig. 9), suggesting that the effect is generic for discrete charge distributions. It is also worth emphasizing that the interaction potential $V(r)$ for $Z=6$ and high salt concentrations [this corresponds to run 9 in Fig. 9(a)] is totally attractive over the whole range of the protein-protein separations.

Once the effective potential $V(r)$ is known, it is straightforward to calculate the second osmotic virial coefficient using Eq. (8). In doing so, however, one should keep in mind that it is the total interaction that enters B_2. Real proteins also exhibit an additional short-range interaction, as seen, for example, in experimental studies of the osmotic pressure and structural data for lysozyme [78], or in fits to its phase behavior [15]. This attraction stems from hydration forces, van der Waals interactions, and other molecular interactions that are, to a first approximation, independent of salt concentration. Hence, we have taken the expected short-range attraction between proteins into account by adding to the effective Coulomb potential in Eq. (9), an additional "sticky" hard sphere potential (SHS) of the Baxter form [39],

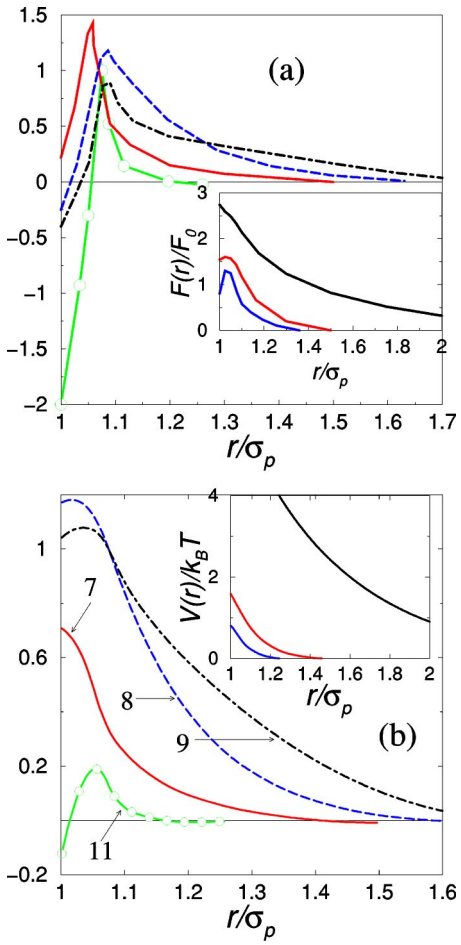

FIG. 8. Total interaction force $F(r)$ (a) and interaction potential $V(r)$ (b) versus dimensionless separation distance r/σ_p for the DCM at $Z=10$. Full curves, run 7; dashed curves, run 8; dash-dotted curves, run 9; full curves with circles, run 11. The inset shows low salt concentrations, from top to bottom, runs 1, 4, 5.

$$\frac{V_{SHS}(r)}{k_BT}=\begin{cases}\infty, & r\leqslant\sigma_p\\ \ln\left[\dfrac{12\tau\delta}{\sigma_p+\delta}\right], & \sigma_p<r<\sigma_p+\delta\\ 0, & r\geqslant\sigma_p+\delta,\end{cases} \qquad (13)$$

with potential parameters $\delta=0.02\sigma_p$ and $\tau=0.12$, which yield reasonable osmotic data for lysozyme solutions [15,26,78] in the high salt concentration regime. This square well potential is isotropic and ignores the directionality in hydrophobic attraction between proteins [33,43]. The second virial coefficient for the SHS potential is

$$\frac{B_2^{(HS)}}{B_2^{(SHS)}}=1-\frac{1}{4\tau}+3\frac{\delta}{\sigma_p}+O\left(\frac{\delta^2}{\sigma_p^2}\right). \qquad (14)$$

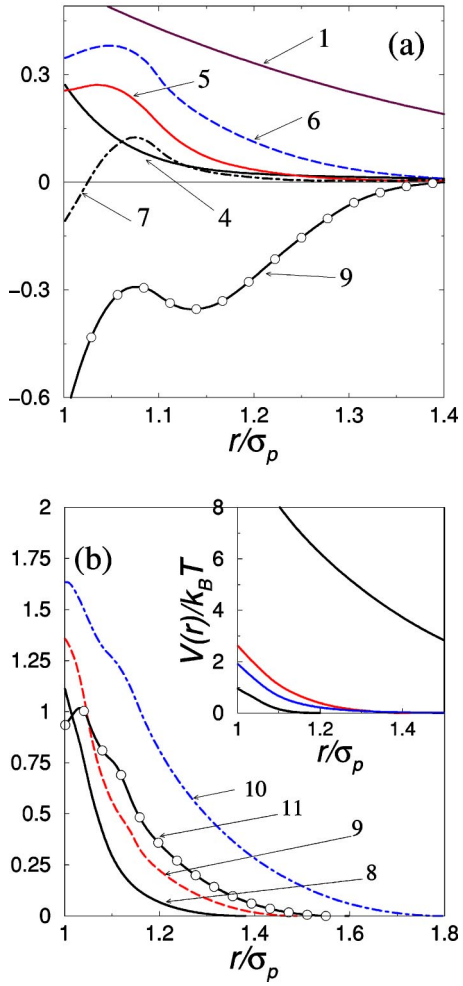

FIG. 9. The same as in Fig. 8 but now for protein charges (a) $Z=6$ and (b) $Z=15$. The run numbers are placed next to corresponding curves. The result for run 1 in (a) is reduced four times to fit the y-axis scale. The inset in (b) shows low salt concentrations, from top to bottom, runs 1, 4, 5, 7.

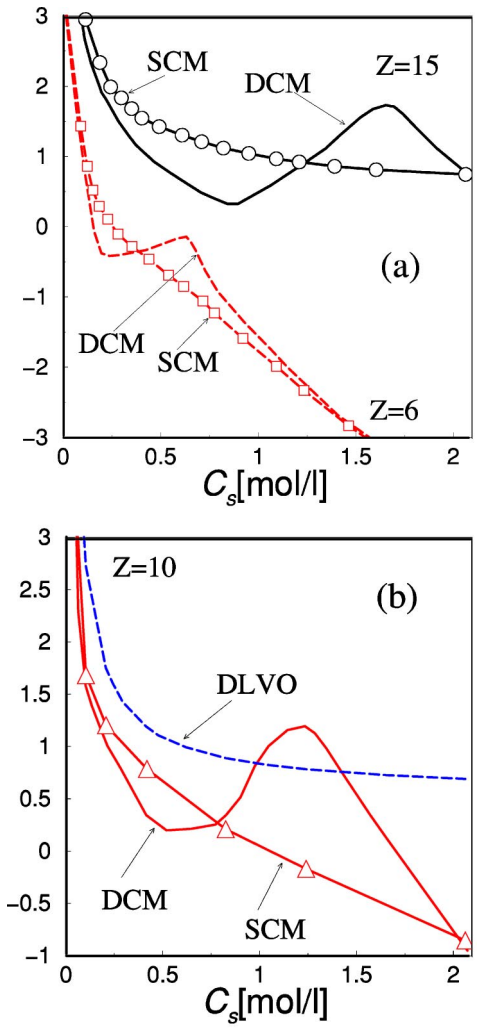

FIG. 10. Normalized second virial coefficient $B_2^*=B_2/B_2^{(HS)}$ of a protein solution versus salt concentration C_s. The lines with (without) symbols correspond to the SCM (DCM) model. In (a) the results are shown for protein charges $Z=6$ (dashed lines) and $Z=15$ (solid lines). Results for $Z=10$ are given in (b) together with a normalized second virial coefficient corresponding to the DLVO potential. Whereas the SCM virial coefficients decrease monotonically with increasing salt concentration, as expected from simple screening arguments, the DCM shows a marked *nonmonotonic* increase of B_2 at intermediate salt concentrations.

Short-range attractions lead to ''energetic fluid'' behavior [79], where the crystallization is driven primarily by the details of the interactions, instead of being dominated by the usual entropic hard-core exclusions. This suggests that the directionality may be very important for details of the protein crystallization behavior [43]. However, for the physically simpler behavior of the virial coefficient, the directionality can be ignored in a first approximation. For simplicity, we assume the parameter τ to be independent of electrolyte conditions, although a weak dependence based on experimental observations is reported in Refs. [26,77]. The addition of $V_{SHS}(r)$ strongly magnifies the nonmonotonicity of B_2 stemming from the nonmonotonic behavior of $V(r)$ near contact.

Results for B_2^* as a function of salt concentration are shown in Fig. 10 for three different protein charges [80]. There is a considerable *qualitative* difference between the predictions of the SCM and the DCM models for the variation of B_2^* with monovalent salt concentration C_s for each protein charge Z. Whereas the SCM (curves with symbols in Fig. 10) predicts a monotonic decay of B_2^* with C_s, the DCM leads to a markedly nonmonotonic variation, involving an initial decay towards a minimum (salting out) followed by a subsequent increase to a maximum (salting in) and a final decrease at high C_s values (salting out). The location of the local minima shifts to higher or lower values of C_s for larger or smaller protein charges Z. Thus, for larger protein charge one needs a higher salt concentration to achieve the ''salting-out'' conditions conducive to protein crystallization [41]. Even though the effective Coulomb potential between proteins is weak, with an amplitude of the order of the thermal energy k_BT, its effect on B_2 is dramatically enhanced by the presence of the strong short-range attractive Baxter potential. We remark that the nonmonotonicity in B_2 occurs at the same salt concentrations in the absence of the short-ranged

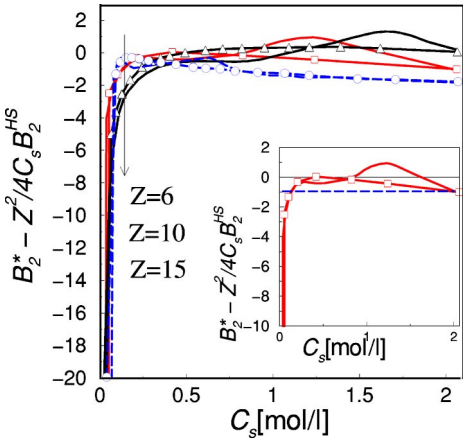

FIG. 11. The same data as in Fig. 10 are shown here for the bare virial coefficient defined by $[B_2-Z^2/4C_s]/B_2^{(HS)}$. The arrow is a guide to the eye for the direction of increasing protein charge Z. The scaling collapse at high C_s has been related to a Donnan equilibrium effect [81]. In the inset, results for the DCM (solid line) and SCM (symbols) for $Z=10$ are compared with the result corresponding to the sticky hard sphere potential, Eq. (14), alone (dashed lines).

attraction; but the difference between the maximal and minimal B_2 in this case is only about 10% as compared to the data of Fig. 10. Different short-range potentials would just lead to different levels of enhancement but would not lead to qualitative changes.

It has recently been proposed [41] that the following ''bare'' second osmotic virial coefficient of protein solutions should be independent of the protein charge Z and the salt concentration C_s, for not too low C_s, namely,

$$B_2^{(0)}=B_2-Z^2/4C_s. \tag{15}$$

This remarkable scaling, which has been observed for a number of experimental conditions [41], may be explained by simple arguments based on Donnan equilibrium [81]. As shown, for example, in Fig. 1 of Ref. [81], this simple relation holds remarkably well above a salt concentration of $C_s \approx 0.25\ M$ for a wide range of experimental measurements of B_2 for lysozyme, which all tend to a plateau value of $B_2^0/B_2^{(HS)} \approx (-2.7 \pm 0.2)$. One implication of this observed scaling is that the attractive interactions that govern $B_2^{(0)}$ are indeed roughly independent of salt concentrations above $C_s \approx 0.25\ M$. When the same scaling procedure is applied to our B_2 curves, a similar plateau develops for both the DCM and the SCM models, albeit with $B_2^{(0)}$ less negative than that found in the experiments, as seen in Fig. 11. The inset to Fig. 11 shows that the bare SCM and DCM second virial coefficients for $Z=10$ go over to a plateau value determined by the ''sticky sphere'' result (14).

One could, of course, very easily match our data with experiments by adjusting the value of τ, but in keeping with our earlier work [50] this is not attempted here. Clearly the scaling does bring the DCM and SCM B_2's close together for a given Z, but for different Z the scaling collapse is not as good as that seen in experiments, since it sets in only at larger C_s. Nevertheless, considering the high density of coions and counterions in the simulation, it is remarkable that a simple Donnan argument based on ideal gas terms performs so well.

The origin of the nonmonotonic variation of B_2^* with C_s can be traced back to the subtle correlation effects which cause an enhancement of the effective Coulomb repulsion at intermediate salt concentrations in the DCM. These effects cannot be rationalized in terms of simple mean-field screening arguments [54]. The protein-microion correlations are of a different nature than those in the SCM, where they lead to a much more conventional, monotonic decay of B_2 with C_s, similar to that expected from a simple screening picture. We emphasize that the observed nonmonotonicity is unrelated to the mutual protein orientations illustrated in Fig. 7. It is explicitly shown in Fig. 7(b) that mutual orientations have a significant influence on the interaction force at small separation distances $r<1.025\sigma_p$. However, Fig. 8(a) reveals that the range of distances where a nonmonotonicity of the interaction force versus added salt is apparent is fairly beyond the distance $r \simeq 1.1\sigma_p$. Thus, the interaction force is nonmonotonic versus added salt at distances about 8 Å from the protein surface, where the influence of mutual protein orientations is negligible. The relatively long-range behavior (as compared to the linear Debye screening length r_D) of the nonmonotonicity of the force versus added salt is entailed by the strong coupling between protein surface charge and salt ions in the DCM model and correlations between the electric double layers associated with these surface charges. Such correlations could result in long-range interactions, due, e.g., to an overcharging effect (see Ref. [82]).

In order to gain further insight into the physical mechanism responsible for the unusual variation of the effective interaction potential and of B_2 with salt concentration in the DCM, we consider the influence of a second nearby protein on the microion distribution close to a central protein. We have computed the difference between ''inner'' and ''outer'' shell microion contact densities for $Z=10$, as schematically illustrated in the inset in Fig. 12. The local microion density is no longer spherically symmetric, due to the interference of the electric double layers associated with the two proteins. The difference $\Delta\rho=\rho_{in}-\rho_{out}$ between the mean number of microions within a fraction of a spherical shell of radius $R=0.6\sigma_p$ subtended by opposite 60° cones, is plotted in Fig. 12 versus salt concentration. $\Delta\rho$ is always positive, indicating that microions (mainly counterions) tend to cluster in the region between the proteins, rather than on the opposite sides. This may be understood because the counterions can lower the total electrostatic energy by being shared between two proteins. However, there is a very significant difference in the variation of $\Delta\rho$ with salt concentration C_s, between the SCM and the DCM models. Both exhibit similar behavior for lower salt concentrations $C_s \leqslant 0.5$ mol/l; for example, both show a small maximum around 0.2 mol/l. But for salt concentrations above 0.5 mol/l, the SCM predicts a monotonic decrease of $\Delta\rho$, while the DCM leads to a sharp peak in $\Delta\rho$ for $C_s \simeq 1$ mol/l. This highly nonmonotonic behavior clearly correlates with the nonmonotonicity observed in Figs. 8–10. The basic mechanism can be summarized as follows:

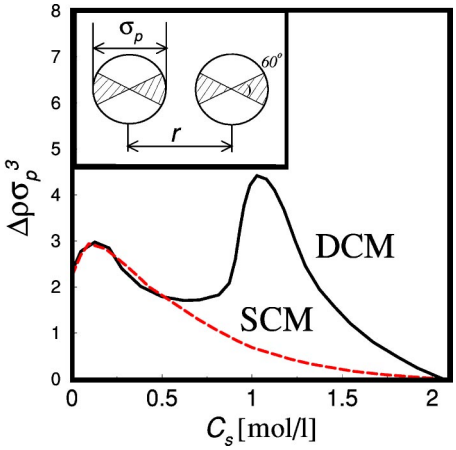

FIG. 12. Difference in the microion densities between and outside two proteins near contact, $\Delta\rho$, versus salt concentration for protein charge $Z=10$ at a protein-protein separation of $r=1.2\sigma_p$. The solid and dashed lines correspond to the DCM and SCM models, respectively. The inset shows the angular range over which $\Delta\rho$ is averaged (see text). The nonmonotonic density profile for the DCM lies at the origin of the nonmonotonic behavior seen for the forces, potentials, and virial coefficients calculated for this model.

For the DCM, the excess number of microions between the two proteins leads to an excess entropic pressure or force, as demonstrated in Fig. 13, which is the origin of the increased *repulsion* between proteins around $C_s=1$ mol/l. The enhanced microion density arises from subtle crowded charge correlation effects that cannot easily be understood at a mean-field level. It was suggested in Ref. [32] that such an enhancement of the cation density around lysozyme at higher salt concentrations could increase the net protein charge and lead to nonmonotonicity in the lysozyme solubility.

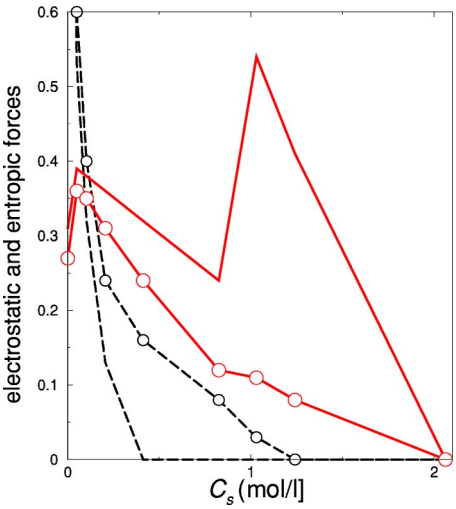

FIG. 13. The electrostatic (dashed lines) and entropic (solid lines) components of the protein-protein interaction force at a protein-protein separation $r=1.2\sigma_p$, in units of k_BT/λ_B, versus salt concentration C_s, for a protein charge of $Z=10$. Lines with or without symbols correspond to SCM or DCM results. This figure demonstrates that the difference between the two models arises primarily from the contributions of the entropic force.

V. CONCLUSIONS

In conclusion, we have calculated the effective interactions and the second osmotic virial coefficient B_2 of protein solutions incorporating the electrostatics within the ''primitive'' model of electrolytes. In this way, we include nonlinear screening, overscreening, and correlation effects missed within the standard Poisson-Boltzmann description. For discrete charge distributions, the interactions and related B_2 vary in a nonmonotonic fashion with increasing ionic strength, while for the smeared charge model, a standard workhorse of colloidal physics, this effect is absent. These correlation-induced effects are missed within nonlinear PB theory, and similar coarse-graining techniques taken from the theory of colloids. In addition to this, our simulations indicate *the necessity of taking entropic forces into account* when treating systems on the nanoscale. These forces are believed to be essential in the salting-out effect [73,83] and could lead to an attraction even between neutral globular proteins [28,84].

Our MD calculations can easily be extended to the more complex (pH dependent) charge patterns of realistic proteins [85]. In fact, in some cases it may be easier to do a full MD simulation than to solve the nonlinear PB equations in a very complicated geometry. We expect mechanisms similar to those found for the DCM to carry over to the more realistic protein models, leading, for example, to an enhanced protein-protein repulsion at intermediate salt concentration. Since the second osmotic virial coefficient determines much of the excess (nonideal) part of the chemical potential of semidilute protein solutions, we expect the nonmonotonicity of B_2 to have a significant influence on protein crystallization from such solutions in the course of a ''salting-out'' process. The nonmonotonic behavior also suggests the possibility of an inverse, ''salting-in'' effect, whereby a reduction of salt concentration may bring B_2 into the ''crystallization slot'' [3,12]. The sensitivity of B_2 to ion-correlation effects may help to explain the salt specificity of the Hofmeister series [73]. Finally, we stress that our nonmonotonicity is qualitatively different from that observed for added nonadsorbing [86,87] and adsorbing [88] polymers or that which result from incorporating repulsive hydration forces at higher salt concentrations [23,24].

ACKNOWLEDGMENTS

The authors are grateful to R. Piazza, I. L. Alberts, P. G. Bolhuis, G. Bricogne, J. Clarke, S. Egelhaaf, J. F. Joanny, D. Rowan, R. Blaak, and W. C. K. Poon for useful discussions; and to the German Science Foundation (DFG), Schlumberger Cambridge Research, and the Isaac Newton Trust for financial support.

[1] S.D. Durbin and G. Feher, Annu. Rev. Phys. Chem. **47**, 171 (1996).
[2] A. Tardieu, A. Le Verge, M. Malfois, F. Bonneté, S. Finet, M. Riés-Kautt, and L. Belloni, J. Cryst. Growth **196**, 193 (1999).
[3] A. George and W. Wilson, Acta Crystallogr., Sect. D: Biol. Crystallogr. **D50**, 361 (1994); A. George, Y. Chiang, B. Guo, A. Arabshahi, Z. Cai, and W.W. Wilson, Methods Enzymol. **276**, 100 (1997).
[4] F. Rosenberger, P.G. Vekilov, M. Muschol, and B.R. Thomas, J. Cryst. Growth **168**, 1 (1996).
[5] R. Piazza, Curr. Opin. Colloid Interface Sci. **5**, 38 (2000).
[6] K.A. Dill, Nature (London) **400**, 309 (1999).
[7] S. Tamashima, Biopolymers **58**, 398 (2001).
[8] B.V. Derjaguin and L.D. Landau, Acta Physicochim. URSS **14**, 633 (1941); E. J. W. Verwey and J.T.G. Overbeek, *Theory of the Stability of Lyophobic Colloids* (Elsevier, Amsterdam, 1948).
[9] G.M. Kepler and S. Fraden, Phys. Rev. Lett. **73**, 356 (1994).
[10] A.E. Larsen and D.G. Grier, Nature (London) **385**, 230 (1997).
[11] R. Verma, J.C. Crocker, T.C. Lubensky, and A.G. Yodh, Phys. Rev. Lett. **81**, 4004 (1998).
[12] D.F. Rosenbaum and C.F. Zukoski, J. Cryst. Growth **169**, 752 (1996).
[13] Y.U. Moon, R.A. Curtis, C.O. Anderson, H.W. Blanch, and J.M. Prausnitz, J. Solution Chem. **29**, 699 (2000).
[14] Y.U. Moon, C.O. Anderson, H.W. Blanch, and J.M. Prausnitz, Fluid Phase Equilib. **168**, 229 (2000).
[15] D. Rosenbaum, P.C. Zamora, and C.F. Zukoski, Phys. Rev. Lett. **76**, 150 (1995).
[16] G.A. Vliegenthart and H.N.W. Lekkerkerker, J. Chem. Phys. **112**, 5364 (2000).
[17] M.H.J. Hagen and D. Frenkel, J. Chem. Phys. **101**, 4093 (1994).
[18] M. Muschol and F. Rosenberger, J. Chem. Phys. **107**, 1953 (1997).
[19] M. Malfois, F. Bonneté, L. Belloni, and A. Tardieu, J. Chem. Phys. **105**, 3290 (1996).
[20] P.R. ten Wolde and D. Frenkel, Theor. Chem. Acc. **101**, 205 (1999).
[21] P.M. Tessier, A.M. Lenhoff, and S.I. Sandler, Biophys. J. **82**, 1620 (2002).
[22] N. Sun and J.Y. Walz, J. Colloid Interface Sci. **234**, 90 (2001).
[23] D.N. Petsev and P.G. Vekilov, Phys. Rev. Lett. **84**, 1339 (2000).
[24] M. Manciu and E. Ruckenstein, Langmuir **18**, 8910 (2002).
[25] V.N. Paunov, E.W. Kaler, S.I. Sandler, and D.N. Petsev, J. Colloid Interface Sci. **240**, 640 (2001).
[26] D.F. Rosenbaum, A. Kulkarni, S. Ramakrishnan, and C.F. Zukoski, J. Chem. Phys. **111**, 9882 (1999).
[27] R. Piazza, S. Iacopini, and M. Galliano, Europhys. Lett. **59**, 149 (2002).
[28] J. Wu, D. Bratko, H.W. Blanch, and J.M. Prausnitz, J. Chem. Phys. **111**, 7084 (1999); Phys. Rev. E **62**, 5273 (2000).
[29] M.L. Broide, T.M. Tominc, and M.D. Saxowsky, Phys. Rev. E **53**, 6325 (1996).
[30] V.G. Taratuta, A. Holschbach, G.M. Thurston, D. Blankschtein, and G.B. Benedek, J. Phys. Chem. **94**, 2140 (1990).
[31] T. Arakawa, R. Bhat, and S.N. Timasheff, Biochemistry **29**, 1914 (1990).
[32] P. Benas, L. Legrand, and M. Ries-Kautt, Acta Crystallogr., Sect. D: Biol. Crystallogr. **D58**, 1582 (2002).
[33] C. Haas, J. Drenth, and W.W. Wilson, J. Phys. Chem. B **103**, 2808 (1999).
[34] K. Demoruelle, B. Guo, S. Kao, H.M. McDonald, D. Nikic, S.C. Holman, and W.W. Wilson, Acta Crystallogr., Sect. D: Biol. Crystallogr. **D58**, 1544 (2002).
[35] J.J. Grigsby, H.W. Blanch, and J.M. Prausnitz, J. Phys. Chem. B **104**, 3645 (2000).
[36] B. Guo, S. Kao, H. McDonald, A. Asanov, L.L. Combs, and W.W. Wilson, J. Cryst. Growth **196**, 424 (1999).
[37] F. Bonneté, S. Finet, and A. Tardieu, J. Cryst. Growth **196**, 403 (1999).
[38] R. Piazza, J. Cryst. Growth **196**, 415 (1999).
[39] R.J. Baxter, J. Chem. Phys. **49**, 2770 (1968).
[40] W.C.K. Poon, Phys. Rev. E **55**, 3762 (1997).
[41] W.C.K. Poon, S.U. Egelhaaf, P.A. Beales, A. Salonen, and L. Sawyer, J. Phys.: Condens. Matter **12**, L569 (2000).
[42] B.L. Neal, D. Asthagiri, and A.M. Lenhoff, Biophys. J. **75**, 2469 (1998); B.L. Neal, D. Asthagiri, O.D. Velev, A.M. Lenhoff, and E.W. Kaler, J. Cryst. Growth **196**, 377 (1999).
[43] R.P. Sear, J. Chem. Phys. **111**, 4800 (1999).
[44] A. Lomakin, N. Asherie, and G.B. Benedek, Proc. Natl. Acad. Sci. U.S.A. **96**, 9465 (1999).
[45] E. Allahyarov, I. D'Amico, and H. Löwen, Phys. Rev. Lett. **81**, 1334 (1998).
[46] P. Linse and V. Lobaskin, Phys. Rev. Lett. **83**, 4208 (1999); J. Chem. Phys. **112**, 3917 (2000).
[47] N. Grønbech-Jensen, K.M. Beardmore, and P. Pincus, Physica A **261**, 74 (1998).
[48] J.P. Hansen and H. Löwen, Annu. Rev. Phys. Chem. **51**, 209 (2000).
[49] A. Striolo, D. Bratko, J.Z. Wu, N. Elvassore, H.W. Blanch, and J.M. Prausnitz, J. Chem. Phys. **116**, 7733 (2002).
[50] E. Allahyarov, H. Löwen, J.P. Hansen, and A.A. Louis, Europhys. Lett. **57**, 731 (2002).
[51] H.L. Friedman, *Ionic Solution Theory* (Wiley Interscience, New York, 1962).
[52] T. Erber and G.M. Hockney, Adv. Chem. Phys. **98**, 495 (1997).
[53] F. Carlsson, P. Linse, and M. Malmsten, J. Phys. Chem. B **105**, 9040 (2001).
[54] F. Carlsson, M. Malmsten, and P. Linse, J. Phys. Chem. B **105**, 12189 (2001).
[55] E. Allahyarov, H. Löwen, and S. Trigger, Phys. Rev. E **57**, 5818 (1998).
[56] E. Allahyarov and H. Löwen, Phys. Rev. E **62**, 5542 (2000).
[57] P. Attard, J. Chem. Phys. **91**, 3083 (1989).
[58] J. Piasecki, L. Bocquet, and J.P. Hansen, Physica A **218**, 125 (1995).
[59] J. Lekner, Physica A **176**, 485 (1991); Mol. Simul. **20**, 357 (1998).
[60] C. Tanford and R. Roxby, Biochemistry **11**, 2192 (1972).
[61] L. Belloni and O. Spalla, J. Chem. Phys. **107**, 465 (1997); O. Spalla and L. Belloni, *ibid.* **95**, 7689 (1991).
[62] D.R. Berard, P. Attard, and G.N. Patey, J. Chem. Phys. **98**, 7236 (1993).
[63] A.A. Louis, E. Allahyarov, H. Löwen, and R. Roth, Phys. Rev. E **65**, 061407 (2002).
[64] R.R. Netz, Phys. Rev. E **60**, 3174 (1999).

[65] S. Alexander, P.M. Chaikin, P. Grant, G.J. Morales, P. Pincus, and D. Hone, J. Chem. Phys. **80**, 5776 (1984).
[66] R. Messina, C. Holm, and K. Kremer, Eur. Phys. J. E **4**, 363 (2001); R. Messina, Physica A **308**, 59 (2002).
[67] P.C. Zamora and C.F. Zukoski, Langmuir **12**, 3541 (1996).
[68] S.B. Howard, P.J. Twigg, J.K. Baird, and E.J. Meehan, J. Cryst. Growth **90**, 94 (1988).
[69] F. Rosenberger, S.B. Howard, J.W. Sowers, and T.A. Nyce, J. Cryst. Growth **129**, 1 (1993).
[70] E. Cacioppo and M.L. Pusey, J. Cryst. Growth **144**, 286 (1991).
[71] R. Messina, C. Holm, and K. Kremer, Phys. Rev. Lett. **85**, 872 (2000).
[72] A. Tardieu, F. Bonnete, S. Finet, and D. Vivares, Acta Crystallogr., Sect. D: Biol. Crystallogr. **D58**, 1549 (2002).
[73] R. Piazza and M. Pierno, J. Phys.: Condens. Matter **12**, A443 (2000).
[74] D. Stigter, Biopolymers **46**, 503 (1998).
[75] J.J. Delrow, J.A. Gebe, and J.M. Schurr, Biopolymers **42**, 455 (1997).
[76] C. Vega and P.A. Monson, J. Chem. Phys. **109**, 9938 (1998).
[77] C.O. Anderson, J.F.M. Niesen, H.W. Blanch, and J.M. Prausnitz, Biophys. Chem. **84**, 177 (2000).
[78] R. Piazza, V. Peyre, and V. Degiorgio, Phys. Rev. E **58**, R2733 (1998).
[79] A.A. Louis, Philos. Trans. R. Soc. London, Ser. A **359**, 939 (2001).
[80] We remark that these data correct those in Ref. [50].
[81] P.B. Warren, J. Phys.: Condens. Matter **14**, 7617 (2002).
[82] J.C.G. Montoro and J.L.F. Abascal, J. Chem. Phys. **103**, 8273 (1995); J.L.F. Abascal and J.C.G. Montoro, *ibid.* **114**, 4277 (2001); S. Gavryushov and P. Zielenkiewicz, Biophys. J. **75**, 2732 (1998); A.P. Lyubartsev and L. Nordenskiöld, J. Phys. Chem. B **101**, 4335 (1997).
[83] V. Vlachy, H.W. Blanch, and J.M. Prausnitz, Adv. Imaging Electron Phys. **39**, 215 (1993); C.J. Coen, H.W. Blanch, and J.M. Prausnitz, *ibid.* **41**, 996 (1995).
[84] F. Bonnete, S. Finet, and A. Tardieu, J. Cryst. Growth **196**, 403 (1999).
[85] M. Boyer, M.-O. Roy, M. Jullien, F. Bonnetè, and A. Tardieu, J. Cryst. Growth **196**, 185 (1999).
[86] A.M. Kulkarni, A.P. Chatterjee, K.S. Schweizer, and C.F. Zukoski, Phys. Rev. Lett. **83**, 4554 (1999).
[87] E. Eisenriegler, J. Chem. Phys. **113**, 5091 (2000).
[88] L.V. Zherenkova, D.A. Mologin, P.G. Khalatur, and A.R. Khokhlov, Colloid Polym. Sci. **276**, 753 (1998).